

# Lattice All-Pass Filter based Precoder Adaptation for MIMO Wireless Channels

Parth Mehta<sup>†</sup>, Agulla Surya Bharath, Kumar Appaiah *Member, IEEE*, Rajbabu Velmurugan *Member, IEEE*, Debasattam Pal *Member, IEEE*

**Abstract**—Modern 5G communication systems employ multiple-input multiple-output (MIMO) in conjunction with orthogonal frequency division multiplexing (OFDM) to enhance data rates, particularly for wideband millimetre wave (mmW) applications. Since these systems use a large number of subcarriers, feeding back the estimated precoder for even a subset of subcarriers from the receiver to the transmitter is prohibitive. Moreover, such frequency domain approaches also do not exploit the predominant line-of-sight component that is present in such channels to reduce feedback. In this work, we view the precoder in the time domain as a matrix all-pass filter, and model the discrete-time precoder filter using a matrix-lattice structure that aids in reducing the overall feedback while still maintaining the desired frequency-phase delay profile. This provides an efficient precoder representation across the subcarriers using fewer coefficients, and is amenable to tracking over time with much lower feedback than past approaches. Compared to frequency domain geodesic interpolation, Givens rotation based parameterisation, and the angle-delay domain approach that depends on approximate discrete-time representation, the proposed approach yields higher achievable rates with a much lower feedback burden. Via extensive simulations over mmW channel models, we confirm the effectiveness of our claims, and show that the proposed approach can reduce the feedback burden by up to 70%.

**Index Terms**—Precoder, Matrix Lattice Filter, Subspace Nevanlinna-Pick Interpolation, 5G, MIMO

## I. INTRODUCTION

Multiple-input multiple-output (MIMO) based wireless communication systems have become the mainstay of several modern wireless communication systems. In conjunction with orthogonal frequency division multiplexing (OFDM), MIMO has enabled the development of scalable high-speed wireless systems. The 5G and beyond 5G standards that are targeted to meet enhanced data rate requirements, largely use high-frequency carrier (millimetre wave (mmW), terahertz (THz) etc.) with wideband OFDM and larger antenna arrays (massive MIMO), along with smart algorithms to increase degrees-of-freedom [1–3]. An essential ingredient in achieving high rates over such links is to use precoding to direct signals effectively in the spatial domain. Effective precoding across all subcarriers for such a system requires channel state information (CSI) to be made available at the transmitter, typically through a limited feedback link from the receiver. Nearly, all current feedback techniques for these systems use frequency domain CSI, which places a large burden on the feedback channel in the wideband MIMO scenario that is fast becoming the norm

in modern wireless communication systems. In this paper, we discuss a more structured feedback approach that uses efficient time-domain realisation of matrix all-pass filters to significantly reduce the feedback requirement without compromising achievable rates. We further show that exploiting temporal correlations of the time varying channel enables tracking of the precoders across all subcarriers with very little incremental feedback.

Precoding in MIMO systems has been studied significantly in the past, and is also part of several standards. Because of the larger array size, we restrict ourselves to the linear precoding schemes, since they are advantageous over non-linear methods in terms of performance and computation cost. In [4], a comprehensive survey of linear precoding techniques for massive MIMO systems is covered. Several precoding techniques such as Maximum Ratio Transmission (MRT), Zero-Forcing (ZF), Minimum Mean Square Error (MMSE), Truncated Polynomial Expansion (TPE), matrix decomposition based methods (like QR decomposition and singular value decomposition (SVD)) influence precoder choice and design [1]. State-of-the-art approaches to precoder design, targeted for 5G related MIMO applications. Precoder design and use in established 5G channel models like 3GPP SCM, WINNER-II that are suitable for specific scenarios are discussed in [2, 3, 5–11]. More generalised models that incorporate massive MIMO, V2V, HST and mmW small-scale fading models for 5G and beyond 5G applications have also seen research interest lately [12, 13].

Typically, the frequency division duplex (FDD) based systems consider the channel matrix in the frequency domain for processing, and the precoding is done for every subcarrier separately. A major drawback here would be huge burden on the receiver to feed back the full or partial CSI across a multitude of subcarriers in wideband communication systems. Since feeding back precoders for all subcarriers is restrictive, particularly for wideband systems, most practical deployments feed back the precoder only for certain subcarriers called pilot subcarriers, while the remaining precoders are interpolated. Interpolating precoders typically exploit the unitary structure of the precoder, and use either manifold based techniques [14, 15], or parameterisation of the precoders and interpolation of these parameters [16]. All these approaches do not necessarily exploit any potential structure that the realisation of the precoder as a filter [in the form of a linear constant coefficient difference equation (LCCDE)] may offer. The concept of time-domain precoding for SISO systems has been considered in the past [17], and this has further led to discussions on time-

domain precoding for MIMO systems [18], wherein it is suggested that the channel impulse response  $\mathbf{H}[n]$  be computed from the frequency-domain channel matrix  $\mathbf{H}(e^{j\omega})$ , and only a few non-zero taps of this impulse response that have comparatively higher channel gain be used to compute the precoding matrix. However, it is yet to be established that time-domain approach offer improved performance when compared to the conventional frequency domain based methods. There are several 5G and beyond 5G channels, wherein the precoder, as a function of frequency, exhibits a structure that can be better captured if expressed in the time-domain, thus leading to improved quantisation. We expand on this approach, with the following contributions:

- The realisation of lattice based matrix all-pass filters is well known for the case of real coefficients [19–22]. We extend this to the case of complex coefficient based filters, since this is necessary to capture precoders for complex baseband channels.
- We extensively use the lattice based matrix all-pass filter (time-domain) representation to capture the precoders for all subcarriers. We show that the time domain realisation is able to capture the precoders' characteristics using very few coefficients. We compute the linear constant-coefficient difference equation (LCCDE) form using subspace Nevanlinna-Pick interpolation (SNIP) approach [23] and then convert them to lattice coefficients. In addition, the lattice approach consists of simple parameters that can easily be tracked, while also ensuring the stability of the realised filter. This also has the distinct advantage of capturing the precoder characteristics across the complete bandwidth of operation, unlike other approaches that capture the approximate filter characteristics using only a few dominant-path components [18, 24].
- Through extensive simulations, we verify that the proposed approach is effective in capturing the wide band precoder, and is amenable to effective tracking over time to yield high data rates. For several 5G channel models, the proposed method is comparable to the traditional frequency-domain based quantisation.

The rest of this paper is organised as follows: Section II shows the formulation of channel model, channel adaptation, and method to calculate achievable rates for a given precoding scheme. Section III explains how to realise the precoder matrix for the wireless MIMO channel model in LCCDE form, and convert it into lattice structure, as well as the advantages of the matrix lattice realisation in terms of stability, quantisation, and adaptability. Section IV shows the quantitative comparison of achievable rates between the geodesic [25], Givens rotation [26, 27] and lattice implementations for various time-varying channel models. Finally, Section V summarises and concludes the proposed method.

## II. SYSTEM MODEL AND ACHIEVABLE RATES

### A. Channel model

We consider a typical MIMO-OFDM discrete-time baseband channel model, as below:

$$\mathbf{y}_t(e^{j\omega}) = \mathbf{H}_t(e^{j\omega})\mathbf{x}_t(e^{j\omega}) + \mathbf{w}_t(e^{j\omega}), \quad \omega \in (-\pi, \pi] \quad (1)$$

where  $\mathbf{x}_t$  and  $\mathbf{y}_t$  are the transmitted and received signals, respectively,  $\mathbf{H}_t$  is the complex channel matrix, and  $\mathbf{w}_t$  is additive white Gaussian noise. Note that all the components mentioned here are functions of frequency  $\omega$ , and varying with time  $t$ . Denoting the  $k$ th sub-carrier frequency by  $\omega_k$ ,

$$\mathbf{y}_t[k] = \mathbf{H}_t[k]\mathbf{x}_t[k] + \mathbf{w}_t[k] \quad (2)$$

Equivalently in the time-domain,

$$\tilde{\mathbf{y}}_t[n] = \tilde{\mathbf{H}}_t[n] * \tilde{\mathbf{x}}_t[n] + \tilde{\mathbf{w}}_t[n] \quad (3)$$

where  $*$  denotes convolution. The channel matrix  $\mathbf{H}_t$  is of size  $N_R \times N_T$ , where  $N_T$  and  $N_R$  represents number of transmit and receive antennas. Here,  $\mathbf{x}_t(e^{j\omega})$ ,  $\mathbf{y}_t(e^{j\omega})$ ,  $\mathbf{H}_t(e^{j\omega})$  are discrete-time Fourier transforms of  $\tilde{\mathbf{x}}_t[n]$ ,  $\tilde{\mathbf{y}}_t[n]$ ,  $\tilde{\mathbf{H}}_t[n]$  at any given time  $t$ , respectively. We compute the frequency response of such a channel  $\mathbf{H}_t(e^{j\omega})$  from a power-delay profile. Given the matrix taps  $[\mathbf{H}_t[0], \mathbf{H}_t[1], \dots, \mathbf{H}_t[L]]$  and the relative delay  $[\tau_{t0}, \tau_{t1}, \dots, \tau_{tL}]$  of each component,  $\mathbf{H}_t(e^{j\omega})$  can be obtained as

$$\mathbf{H}_t(e^{j\omega}) = \sum_{l=0}^L \mathbf{H}_t[l] e^{-j\omega\tau_{tl}}. \quad (4)$$

The channel  $\mathbf{H}_t$  considered here is slowly varying, and is modelled using an AR(1) process as shown in (5) [28]. Each element  $[\mathbf{H}_t]_{ij}$  in the channel matrix  $\mathbf{H}_t$  is modelled as

$$[\mathbf{H}_t[n]]_{ij} = \alpha_{ij} [\mathbf{H}_{t-1}[n]]_{ij} + \sqrt{1 - \alpha_{ij}^2} [\mathbf{W}_t[n]]_{ij} \quad (5)$$

where  $\mathbf{H}_{t-1}$  is the channel at previous time instant,  $[\mathbf{W}_t]_{ij} \sim \mathcal{N}(0, 1)$ , and  $\alpha_{ij} \in (0, 1)$ . The value of  $\alpha$  is chosen to reflect the rate of channel variation, as in (6) [28].

$$\alpha = J_0(2\pi f_d T_s) \quad (6)$$

where  $J_0(\cdot)$  is the 0th order Bessel function,  $f_d = \frac{v}{c} F_c$  is the relative Doppler frequency, given the carrier frequency  $F_c$ , speed  $v$  and the speed of electromagnetic waves in free-space  $c$ ; and  $T_s$  is the symbol duration.

### B. Optimal Precoding and Achievable Rates

The transmit vector  $\mathbf{x}_t$  in a MIMO-OFDM setup is typically precoded. The purpose of this precoder is to maximise the overall achievable rate for a given channel  $\mathbf{H}_t$ . Denoting the precoder as  $\mathbf{P}_t$ , the transmit vector for the  $k$ th subcarrier can be given as

$$\mathbf{x}_t[k] = \mathbf{P}_t[k]\mathbf{d}_t[k], \quad k = 0, 1, \dots, N_{\text{FFT}} - 1 \quad (7)$$

where  $\mathbf{d}_t$  is the data, and  $N_{\text{FFT}}$  is the number of subcarriers.

To obtain the optimal achievable rate for a linear receiver, the precoder  $\mathbf{P}_t$  is the matrix of right singular vectors of the channel matrix  $\mathbf{H}_t$  [29]. Hence, for every subcarrier  $k$ ,

$\mathbf{P}_t[k] = \mathbf{V}_t[k]$ , and  $\mathbf{H}_t[k] = \mathbf{U}_t[k]\mathbf{\Sigma}_t[k]\mathbf{V}_t^H[k]$  as shown in Fig. 1, where  $\mathbf{\Sigma}_t[k]$  is a diagonal matrix consisting of the singular values of  $\mathbf{H}_t[k]$ . This precoder is estimated at the receiver, and fed back to the transmitter for all subcarriers.

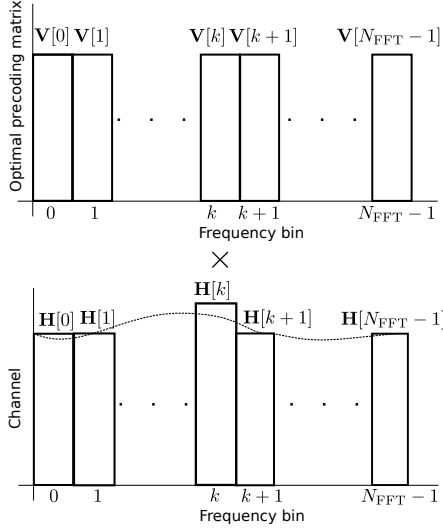


Fig. 1. Abstract representation of approximated magnitudes of OFDM subcarriers for  $N_{\text{FFT}}$  subcarriers.

Now, given the channel  $\mathbf{H}_t$  and precoder  $\mathbf{P}_t$ , the equivalent channel is  $\mathbf{H}_{t_{\text{eq}}} = \mathbf{H}_t \mathbf{P}_t$ . With the zero-forcing (ZF) linear receiver [29, 30] of the form  $\mathbf{Z} = \mathbf{F} \mathbf{H}_{t_{\text{eq}}}^H$ , where  $\mathbf{F} = (\gamma \mathbf{H}_{t_{\text{eq}}}^H \mathbf{H}_{t_{\text{eq}}})^{-1}$ , the achievable rate can be computed as

$$r_{\text{ZF}} = \sum_{k=0}^{N-1} \log_2 \left( 1 + \frac{1}{[\mathbf{F}]_{kk}} \right) \quad (8)$$

where  $N$  is the number of streams (number of diagonal elements of  $\mathbf{F}$ ), and  $[\mathbf{F}]_{kk}$  are the diagonal elements of  $\mathbf{F}$  [29].

### C. Precoder Adaptation

To track the precoder for slowly varying channels shown in Section II-A, adaptive quantisation approaches such as Adaptive-Delta Pulse-Coded Modulation (ADPCM) are typically employed, since they track only the precoder changes, and thus require very little feedback. As shown in [26, 27], to track small changes in a quantity ( $\hat{x}$ ), only 1-bit is sufficient to determine the direction of the update (i.e., positive or negative) of the parameter. This can be done by tracking the sign-bit  $\beta$ . For frequency based methods, this has to be done for every subcarrier (or every pilot subcarrier, if the remaining are interpolated). The approach to track the time-varying parameter  $x_t$  using single bit updates at each time instant can be represented as follows:

$$\hat{x}_t = \hat{x}_{t-1} + \beta_t \mu_t, \text{ where } \mu_t = \begin{cases} \sigma \mu_{t-1} & : \beta_t = \beta_{t-1} \\ \mu_{t-1} / \sigma & : \beta_t \neq \beta_{t-1} \end{cases} \quad (9)$$

where  $\sigma > 1$  is the step size.

In the case of a MIMO-OFDM system that contains a large number of antennas as well as a large number of subcarriers, the amount of data that the receiver has to feedback to the

transmitter is large, even when adaptive feedback is employed. One approach to reduce the amount of feedback is for the receiver to track and feed back precoder updates only for pilot subcarriers, so that the transmitter can interpolate to obtain the precoders at the remaining subcarriers [25]. This method, while effective in several situations, is highly sensitive to the number of pilot subcarriers. This can be attributed to the fact that frequency domain interpolation does not guarantee that the characteristics are satisfied for any frequencies other than the pivot points that are used for interpolation. This issue is exacerbated in the case of matrix filters, since interpolation accuracy suffers significantly when using matrix based filters.

One approach to address this issue is to parameterise the unitary matrices that represent the precoders as scalar parameters using Givens rotations [26]. This approach yields a unique set of scalar parameters that completely capture the characteristics of unitary matrices (such as the precoding matrices) using a set of parameters  $\phi_{k,l}$  and  $\theta_{k,l}$ , as shown in (10). A unitary matrix  $\mathbf{V}_t$  of size  $m \times m$  can be decomposed as follows:

$$\mathbf{V}_t(e^{j\omega}) = \left[ \prod_{k=1}^m \mathbf{S}_k(\phi_{k,k}, \dots, \phi_{k,m}) \prod_{l=1}^k \mathbf{C}_{m-l, m-l+1}(\theta_{k,l}) \right], \quad \forall \omega. \quad (10)$$

Here,  $\mathbf{S}_k(\phi_{k,k}, \dots, \phi_{k,m}) = [\text{diag}(\mathbf{1}_{k-1}, e^{j\phi_{k,k}}, \dots, e^{j\phi_{k,m}})]$  with  $\mathbf{1}_k$  is  $k-1$  ones; and

$$\mathbf{C}_{m-l, m-l+1}(\theta) = \begin{bmatrix} \mathbf{I}_{m-l-1} & & \\ & \cos \theta & -\sin \theta \\ & \sin \theta & \cos \theta \\ & & & \mathbf{I}_{l-1} \end{bmatrix}$$

where the blank entries are all zeros.  $\phi_{k,l}$  and  $\theta_{k,l}$  are referred to as phases and angles of rotations, respectively. This way, the complex precoding matrix  $\mathbf{V}_t$  can be represented compactly using  $m^2$  real scalar parameters  $(\phi_{k,l}, \theta_{k,l})$ , that can be tracked more effectively using (9). However, these parameters are still frequency dependent, and the tracking has to be performed for all or pilot subcarriers. Moreover, directly interpolating the frequency domain parameters may not result in accurate representation of the precoding filter characteristics.

Another estimation approach that is suited for 5G systems employs the angle-delay based channel estimation approach [24]. This approach exploits the sparse nature of the 5G channel in the discrete-time domain to estimate the channel coefficients. Since this method involves estimation of the complete channel, we employ this to find only the precoder while adaptively tracking the temporal variation of the channel coefficients. Because of the restrictions on the amount of information for the feedback, adaptive quantisation has to be applied. A major challenge of using this approach is that it approximates the channel in the discrete-time domain to only a few initial coefficients (channel taps). This, along with adaptive quantisation results in an inaccurate precoder representation, when reconstructing the precoder for all subcarriers at the transmitter end.

In this work, we take the approach of explicitly constructing a matrix all-pass filter and track that filter instead, and we show that the proposed approach requires a smaller number

of parameters to feed back while obtaining achievable rates in excess of those achieved using the geodesic [25], Givens rotations [26, 27], and angle-delay based method [24].

### III. MATRIX LATTICE FILTER

#### A. Time-domain Realisation using SNIP

As discussed in the previous section, there are several issues when using purely frequency domain based interpolation and design techniques for matrix all-pass filters in general. This is particularly applicable to situations wherein an accurate time-domain characterisation of the filter may exist, as is often the case with 5G mmW systems that frequently exhibit a predominant line-of-sight characteristic. In these situations, the time domain characterisation is not only more compact, but can also capture the response of the precoder (when viewed as a matrix filter) more accurately. To this end, we adapt the approach described in [23] to design the precoder as a time-domain filter, as discussed below.

**Theorem 1.** *Given unitary matrices  $\mathbf{V}(e^{j\omega_k})$  and group-delay matrices  $\mathbf{F}(e^{j\omega_k})$ ,  $k \in \{0, \dots, M-1\}$ , there exist polynomials  $\mathbf{N}(z)$  and  $\mathbf{D}(z)$  such that  $\mathbf{V}(e^{j\omega_k}) = \mathbf{N}(e^{j\omega_k})\mathbf{D}^{-1}(e^{j\omega_k})$ , where  $\mathbf{V}$  is obtained from SVD of channel matrix  $\mathbf{H}$ . This is called subspace Nevanlinna-Pick interpolation (SNIP) approach to factorise unitary matrix  $\mathbf{V}(e^{j\omega})$  into rational matrix polynomials  $\mathbf{N}(e^{j\omega})$  and  $\mathbf{D}(e^{j\omega})$ , where  $\mathbf{N}$  and  $\mathbf{D}$  satisfy the following condition:*

$$\begin{aligned} \mathbf{V}^H(e^{j\omega})\mathbf{V}(e^{j\omega}) &= \mathbf{I}_m \\ \mathbf{N}^H(e^{j\omega})\mathbf{N}(e^{j\omega}) - \mathbf{D}^H(e^{j\omega})\mathbf{D}(e^{j\omega}) &= \mathbf{0}_m, \forall \omega \in [-\pi, \pi). \end{aligned}$$

*Proof.* This has been proved in [23].  $\square$

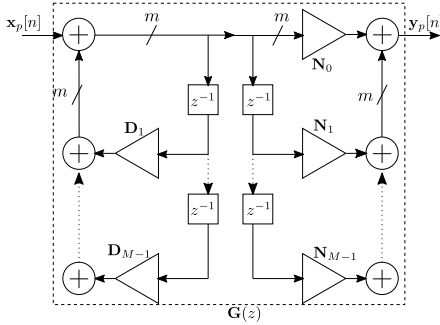


Fig. 2. LCCDE (Direct Form II) implementation of matrix filter with right co-prime factorisation ( $\mathbf{V}(z) = \mathbf{N}(z)\mathbf{D}^{-1}(z)$ ).

The SNIP approach from Theorem 1, ensures that we obtain a *realisable* filter that captures the precoder characteristics, in the sense that  $\mathbf{N}(e^{j\omega})$  and  $\mathbf{D}(e^{j\omega})$  are matrix polynomials that can be used to obtain a LCCDE that precisely satisfies the filter constraints at  $\omega_0, \dots, \omega_{N-1}$  while also guaranteeing that  $\mathbf{N}(e^{j\omega})\mathbf{D}^{-1}(e^{j\omega})$  is unitary for all  $\omega \in [-\pi, \pi)$ . Therefore, if the precoder matrices' frequency domain response can be characterised as a realisable matrix all-pass filter, the SNIP approach is likely to capture this more accurately than a frequency domain interpolation [23]. An additional benefit is that, if the SNIP is performed using only  $M$  points, the

resulting matrix all-pass filter can be realised using  $M$  poles and zeros, that can also be implemented in the time-domain using the Direct Form II as opposed to a frequency domain approach that employs DFT-IDFT operations.

We denote the all-pass filter as  $\mathbf{G}(e^{j\omega})$ , which is the precoding matrix  $\mathbf{V}(e^{j\omega})$ .  $\mathbf{x}_p$  and  $\mathbf{y}_p$  are respectively the input and output of the precoder  $\mathbf{G}$ . Fig. 2 depicts this filter with Direct Form II realisation. Here,

$$\mathbf{N}(e^{j\omega}) = \sum_{i=0}^{M-1} \mathbf{N}_i e^{-ij\omega}, \quad \mathbf{D}(e^{-j\omega}) = \sum_{i=0}^{M-1} \mathbf{D}_i e^{-ij\omega}, \quad (11)$$

where  $\mathbf{N}_k, \mathbf{D}_k, k = 0, 1, \dots, M-1$  are matrices, and  $\mathbf{D}_0 = \mathbf{I}_m$ . Although the Direct Form II is an effective way of realising a discrete-time filter, there exist certain limitations in this representation for our application, as listed below.

- 1) When transforming the filter representation from frequency-domain to time-domain realisation, the stability of the filter becomes important, even for an all-pass filter. For scalar all-pass filters, an explicit relationship exists between the numerator and denominator polynomials (as discussed in Section III-C) that ensures the filter stability even after quantisation. Unfortunately, for the matrix all-pass filter case, there is no such direct relation between  $\mathbf{N}(e^{j\omega})$  and  $\mathbf{D}(e^{j\omega})$  polynomials. Hence, it becomes difficult to comment on the stability directly from these coefficients.
- 2) Because of the absence of a “convenient” structure for  $\mathbf{N}(e^{j\omega})$  and  $\mathbf{D}(e^{j\omega})$ , directly tracking the filter coefficients while preserving the unitary nature of  $\mathbf{G}(e^{j\omega})$  and its stability are also difficult.

To address these limitations, we propose the use of lattice structures to represent  $\mathbf{G}(e^{j\omega})$  instead of the Direct Form II realisation. For simplicity of derivation, we consider all inputs and outputs are of same dimensions  $m$ , which implies we will only deal with  $m \times m$  square matrices, although these techniques are extensible to the case of non-square precoders as well using approaches similar to those discussed in [26]. We will also use  $z$  instead of  $e^{j\omega}$  to represent all the matrix polynomials in terms of the general complex argument  $z$ .

#### B. Lattice Structure Realisation

To understand the lattice realisation for the matrix all-pass filter, we first look into the scalar case. The transfer function of a stable scalar all-pass filter can be given as

$$H_d(z) = \frac{N_d(z)}{D_d(z)} = \frac{z^{-d} D_d^*(1/z^*)}{D_d(z)} \quad (12)$$

where  $d$  is the polynomial degree and  $(\cdot)^*$  denotes the complex conjugate [19]. Since the filter is stable, the roots of  $D_d(z)$  (poles of  $H_d(z)$ ) lie inside the unit-circle in the complex  $z$ -plane. One can synthesise the lattice structure to realise the given filter of degree  $d$ , in an iterative way, as shown below.

$$z^{-1} H_{k-1}(z) = \frac{H_k(z) - C_{k-d}}{1 - C_{k-d} H_k(z)}, \quad k \in \{d, d-1, \dots, 1\}$$

where  $C_{k-d} = H_k(\infty)$  are the lattice parameters. Since the poles of  $H_d(z)$  lie inside the unit-circle, it can be verified that

$H_{d-1}(z)$  is also stable, and  $|C_k| < 1$  [19]. Therefore, inferring the stability of the filter using the Direct Form implementation (in terms of  $N(z)$  and  $D(z)$ ) requires computation of roots of a  $d$ -degree polynomial, whereas for the lattice realisation, only verifying that  $|C_k| < 1$  is enough. Moreover, it is convenient to adapt and quantise the lattice parameters  $C_k$ , since it combines the effect of adapting and quantising both  $N(z)$  and  $D(z)$ , while ensuring the stability and all-pass nature. These are some of the key advantages of lattice based filter realisations, and these can be adapted effectively to the matrix case to represent the precoder variations across time and frequency efficiently.

The matrix lattice structure can be constructed from the Direct Form II by considering a 2-port system, as shown in Fig. 3, where the output at port-2 ( $y_2$ ) is connected to input at port-2 ( $x_2$ ). The transfer function at port-2 is considered to be of length  $M - 1$  and the overall transfer function is of length  $M$ .

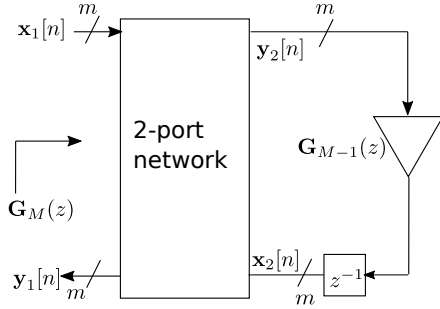


Fig. 3. 2-port representation of lattice filter structure.

The 2-port system can be realised using the transmission parameters (T-parameters) as shown in Fig. 4. Denoting the input and output vectors as  $\mathbf{x}_k(z)$  and  $\mathbf{y}_k(z)$  for  $k = 1, 2$  respectively, we can write

$$\mathbf{y}[n] = \begin{bmatrix} y_1[n] \\ y_2[n] \end{bmatrix} = \begin{bmatrix} \mathbf{T}_{11} & \mathbf{T}_{12} \\ \mathbf{T}_{21} & \mathbf{T}_{22} \end{bmatrix} \begin{bmatrix} x_1[n] \\ x_2[n] \end{bmatrix} = \mathbf{T} \mathbf{x}[n] \quad (13)$$

where  $\mathbf{x}_1[n] = x_p[n]$  and  $\mathbf{y}_1[n] = y_p[n]$ . Similar to scalar lattice filter realisations, at the  $k$ th stage the T-parameters are related to each other and can be characterised by a common matrix  $\mathcal{K}_k$  as shown in (14) [20].

$$\mathbf{T}_k = \begin{bmatrix} \mathcal{K}_k & (\mathbf{I}_m - \mathcal{K}_k \mathcal{K}_k^H)^{\frac{1}{2}} \\ (\mathbf{I}_m - \mathcal{K}_k^H \mathcal{K}_k)^{\frac{H}{2}} & -\mathcal{K}_k^H \end{bmatrix} \quad (14)$$

where  $(\cdot)^{\frac{1}{2}}$  denotes the matrix square root of a complex matrix,  $(\cdot)^{\frac{H}{2}}$  and  $(\cdot)^{-\frac{H}{2}}$  denotes square root and inverse of the square root of the Hermitian transpose of the matrix, respectively;  $\mathcal{K}_k$  is of size  $m \times m$  and  $\mathbf{T}_k$  is of size  $2m \times 2m$ .

As discussed earlier, several limitations exist when implementing the precoding using either the frequency-domain methods discussed in Section II or the Direct Form II implementation listed in Section III-A. To address these, we propose the lattice based realisation, since it addresses the issues with past approaches, as discussed in Section III-C.

We next discuss the approach to obtain the T-parameters from  $\mathbf{N}(z)$  and  $\mathbf{D}(z)$ . Algorithm 1 captures the step-wise process to iteratively obtain the T-parameters. The algorithm largely corresponds to the traditional approach of converting

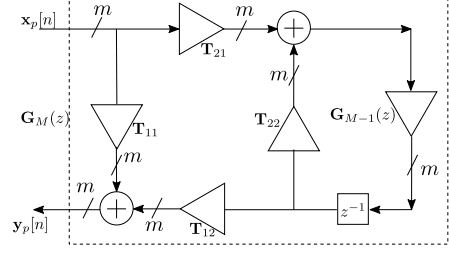


Fig. 4. Realising a single stage of matrix lattice filter using T-parameters.

#### Algorithm 1 Iteratively compute the matrix lattice parameters

Start with unitary  $\mathbf{G}_n(z) = \mathbf{N}_n(z)\mathbf{D}_n(z)^{-1}$ .

**repeat**

Multiply  $\mathbf{N}_n(z)$  and  $\mathbf{D}_n(z)$  by  $\mathbf{D}_0^{-1}$  such that  $\mathbf{D}_0 = \mathbf{D}_n(\infty) = \mathbf{I}_m$ .

$\mathcal{K}_{n-k} = \mathbf{G}_k(\infty) = \mathbf{N}_k(\infty) = \mathbf{N}_0$

Find T-parameters using (14).

Find  $\hat{\mathbf{D}}_n = (\mathbf{T}_{21}^H \mathbf{T}_{21})^{-1} (\mathbf{D}_n(z) - \mathcal{K}_{n-k}^H \mathbf{N}_n(z))$ .

Find  $\hat{\mathbf{N}}_n = \mathbf{N}_n(z) - \mathcal{K}_{n-k} \hat{\mathbf{D}}_n$ .

$\mathbf{D}_{n-1}(z) = \mathbf{T}_{21} \hat{\mathbf{D}}_n$

Remove the last matrix, which will be  $\mathbf{0}_m$ .

$\mathbf{N}_{n-1}(z) = (\mathbf{T}_{12} + \mathcal{K}_{n-k} \mathbf{T}_{21}^{-1} \mathcal{K}_{n-k}^H)^{-1} \hat{\mathbf{N}}_n$

Remove the first matrix which will be  $\mathbf{0}_m$ .

Find  $\mathbf{G}_{n-1}(z) = \mathbf{N}_{n-1}(z)\mathbf{D}_{n-1}(z)^{-1}$ .

**until**  $\mathbf{G}_0(z)$  is reached.

$\mathbf{R} = \mathbf{G}_0(z)$

Direct Form II realisations to lattice structures for scalar filters, with minor differences arising due to the matrix case. We begin with the SNIP based filter that is obtained using Theorem 1, referred to as  $\mathbf{G}_n(z)$ , that yields  $\mathbf{N}_n(z)$  and  $\mathbf{D}_n(z)$ . In each iteration, the algorithm computes one of the  $\mathcal{K}_k$  parameters, and “removes” the contribution of this parameter from the original filter to obtain the all-pass filter  $\mathbf{G}_{n-1}(z)$ , that has order one less than  $\mathbf{G}_n(z)$ . After  $M - 1$  stages, the last remaining polynomial is the residue transfer function ( $\mathbf{R}$ ). Hence, the whole matrix filter can be characterised by  $M$  parameters (viz.  $\mathcal{K}_0, \mathcal{K}_1, \dots, \mathcal{K}_{M-2}$  and one  $\mathbf{R}$ ), as opposed to LCCDE implementation which requires  $2M$  parameters ( $M \mathbf{N}_k$  and  $M \mathbf{D}_k$ ). The overall lattice filter is shown in Fig. 5.

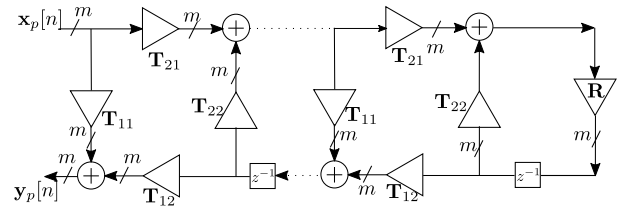


Fig. 5. Overall matrix lattice filter of length  $M$ .

To preserve the unitary nature for each lattice stage, the following conditions should be satisfied:

$$\mathbf{T}_{11}^H \mathbf{T}_{11} + \mathbf{T}_{21}^H \mathbf{T}_{21} = \mathbf{I}_m \quad (15a)$$

$$\mathbf{T}_{12}^H \mathbf{T}_{12} + \mathbf{T}_{22}^H \mathbf{T}_{22} = \mathbf{I}_m \quad (15b)$$

$$\mathbf{T}_{11}^H \mathbf{T}_{12} + \mathbf{T}_{21}^H \mathbf{T}_{22} = \mathbf{0}_m \quad (15c)$$

The proof and conditions for real T-parameters can be adapted from the results in [20] and can be suitably modified for complex T-parameters. Conditions in (15) can be combined into a single condition as

$$\mathcal{T}^H \mathcal{T} = \begin{bmatrix} \mathbf{I}_m & \mathbf{0}_m \\ \mathbf{0}_m & \mathbf{I}_m \end{bmatrix} = \mathbf{I}_{2m}. \quad (16)$$

### C. Advantages of Lattice Realisation

We now discuss how the use of lattice realisations addresses the issues of ensuring stability, adaptability, and easy quantisation of the precoding all-pass filter when compared to the past approaches.

1) *Stability*: Even though precoders are implemented as all-pass filters, ensuring filter stability is essential, since a practical implementation that does not ensure stability could result in saturation and loss in accuracy that could compromise performance significantly. This is even more important in the case where these filters are parameterised and the parameters are tracked, since some parameter updates could cause loss in stability. Verifying the stability of causal filters in general requires computation of roots of the denominator polynomial to ensure that the poles are within the unit circle. This is especially applicable to matrix all-pass filters, wherein it is difficult to infer the stability directly from the filter coefficients  $\mathbf{N}(z)$  and  $\mathbf{D}(z)$ . Explicitly, such an approach would require evaluating all roots of  $\det(\mathbf{D}(z))$  and ensuring that they are all within the unit circle, which is computationally intensive. In contrast, by realising and representing the filter in the lattice form, the lattice parameters  $\mathcal{K}_k$  can directly capture the stability information, much like in the case of scalar lattice structures. The scalar filter is considered to be stable if the lattice parameters for all stages  $C_k$ , satisfy  $|C_k| < 1$ . Similarly, for the matrix filter case, we have [20]:

$$\mathcal{K}_k^H \mathcal{K}_k \prec \mathbf{I} \text{ and } \mathcal{K}_k \mathcal{K}_k^H \prec \mathbf{I} \quad (17)$$

which implies that  $\mathbf{I} - \mathcal{K}_k^H \mathcal{K}_k$  and  $\mathbf{I} - \mathcal{K}_k \mathcal{K}_k^H$  are positive definite matrices. We remark here that we use non-degenerate version of the inequalities mentioned in [20]. This condition also ensures the matrix roots in (14) exist. In other words, all the singular values of  $\mathbf{T}_{ij}$  lie in  $[0, 1]$ , for all stages.

2) *Quantisation*: Another issue with both the frequency based approaches as well as the Direct Form II implementations is that the parameters are not easy to quantise. In the frequency based approach, not capturing the time-domain structure would imply that the precoder should be quantised in the frequency domain for more subcarriers to ensure accuracy of reconstruction, thereby resulting in a much larger feedback burden. In the Direct Form II realisation that can be inferred in a straightforward manner by applying Theorem 1, we note that a useful structure that relates  $\mathbf{N}(z)$  and  $\mathbf{D}(z)$  and is useful for quantisation is absent. As an example, for a scalar all-pass filter, the numerator and denominator polynomials  $N(z)$  and  $D(z)$  are in reverse order and conjugate [19] as shown in (12). Hence, if we were to quantise one set of coefficients, say  $N(z)$ , it directly captures the effect in  $D(z)$  owing to the fact that the absolute value of the filter response on the unit circle is unity.

In addition, directly quantising the coefficients of  $\mathbf{N}(z)$  and  $\mathbf{D}(z)$  could result in a filter that may not be all-pass for all  $z = e^{j\omega}$ . In contrast, when considering the lattice based approach, since each lattice stage is characterised by only one parameter  $\mathcal{K}_k$ , the information fed back from the receiver to the transmitter can be reduced, as we show in Section IV. Moreover, since  $\mathcal{K}_k$  completely parameterise the precoding all-pass filter, the need to track  $\mathbf{N}(z)$  and  $\mathbf{D}(z)$  separately is obviated. In addition, the lattice structure ensures that the resulting filter will be all-pass even when  $\mathcal{K}_k$  are quantised.

To quantise and adapt the  $\mathcal{K}_k$ , we use the approach shown in [26]. For a slowly varying channel  $\mathbf{H}_t$ , the parameters  $\mathcal{K}_k$  also vary slowly, as shown in (5) according to an AR(1) process. Similar to that in (9), we can write the adaptive quantisation of  $\mathcal{K}_k$  for the  $k$ th stage as

$$\hat{\mathcal{K}}_{k_t} = \hat{\mathcal{K}}_{k_{t-1}} + \Delta_{k_t} \Gamma_{k_t}, \quad \text{where } \Gamma_{k_t} = \begin{cases} \sigma \Gamma_{k_{t-1}} & : \Delta_{k_t} = \Delta_{k_{t-1}} \\ \Gamma_{k_{t-1}} / \sigma & : \Delta_{k_t} \neq \Delta_{k_{t-1}} \end{cases} \quad (18)$$

where  $\Delta$  and  $\Gamma$  are complex matrix updates, that correspond to  $\beta$  and  $\mu$  in (9). The comparisons ( $=$  and  $\neq$ ) and multiplication ( $\Delta_{k_t} \Gamma_{k_t}$ ) are element-wise and independent for real and imaginary parts of the complex matrices.  $\sigma$  is chosen such that the entries of  $\mathcal{K}_k$  do not exceed 1, and (17) is satisfied. This ensures that the unitary nature and stability of the lattice realisation is preserved, even after adaptive quantisation.

3) *Adaptability*: As shown in (5), a slowly varying channel  $\mathbf{H}_t[n]$  can be modelled as an AR(1) process. For such channels, it is desired to track the precoding parameters accordingly. This is computationally costly for the previous frequency-domain based methods, where the precoding matrix for every subcarrier has to be tracked. The time-domain realisation helps, as the number of parameters to track ( $\mathbf{N}(z)$  and  $\mathbf{D}(z)$ ) could be less than that for the frequency-domain approach. However, using the lattice structure, the number of parameters can be reduced further (from  $2M$  to  $M$ ), which can potentially make the process faster. Moreover, the *phase-unwrapping* because of  $2\pi$  jumps required [27] in the frequency-domain method can also be avoided. The adaptive quantisation thus explained in the previous section can quantise and adapt to the slowly varying channel by tracking the lattice parameters  $\mathcal{K}$ .

As per (5) and (6), the rate of change is dependent on the relative speed between the transmitter and receiver. For larger speeds, the value of  $\alpha$  is low, which means the correlation between  $\mathbf{H}_t[n]$  and  $\mathbf{H}_{t-1}[n]$  drops, and the tracking parameters  $\Gamma$  and  $\sigma$  in (18) changes accordingly. For typical slow variations in channel,  $\alpha \geq 0.9$ .

## IV. SIMULATION RESULTS AND DISCUSSION

In this section, we present simulation results that quantify the benefit of using the proposed adaptive precoder feedback approach, and compare this with other adaptive precoder feedback methods that are primarily frequency-domain based. We also verify the advantages of the lattice representation of precoders and compare them with the frequency based geodesic [25] and Givens rotation [26, 27] methods.

To model the 5G mmW channel characteristics, we consider the empirical model described in [31] that specifies the power delay profiles for a typical 28 GHz 3D channel model that was verified experimentally. Adapting the parameters described therein appropriately to our scenario, the resulting power-delay profile is shown in TABLE I. The powers are normalised with respect to the first temporal component. This is a wideband

TABLE I  
POWER-DELAY PROFILE OF THE 5G MILLIMETER-WAVE CHANNEL

<b>Normalized Power (dB)</b>	0	-112	-132	-142	-153
<b>Delay (ns)</b>	0	381	407	1433	1500

channel, and the LOS component is dominant while the reflections are very small. For such a channel, a typical approach to precoder design is sub-band-wise [32]. Due to the wideband nature of the channel, the number of OFDM subcarriers is very large so as to ensure that the channel can be considered to be flat fading within a subcarrier. We consider a  $4 \times 4$ ,  $8 \times 8$ ,  $12 \times 12$ , and  $15 \times 15$ , MIMO systems with total 4096 subcarriers. We then consider the 5G New Radio (NR) resource-block (RB) architecture [33], and group 1024 subcarriers to make 4 RB for  $4 \times 4$  and  $8 \times 8$  systems, and group 512 subcarriers to make 8 RB for  $12 \times 12$  and  $15 \times 15$  systems. Unlike the typical RB architecture where the RB consists of only 12 subcarriers, we consider a larger group (1024 and 512) because of the typical nature of the channel as discussed above. The first subcarrier in each RB is considered pilot subcarrier, which represents the whole RB. We then compare the achievable rates with precoding, with the precoder being fed back only for the RBs. In the case of the geodesic interpolation [25] and the scalar parameterisation [26, 27] approaches, the precoder is tracked at these pilot subcarriers, and is interpolated in the frequency domain at the transmitter to construct the complete precoder for all subcarriers. The pilot subcarriers are chosen equi-spaced in the span  $[0, 4095]$ . For the angle-delay domain precoder tracking, we first take an inverse Fourier transform of the precoder, which gives an equivalent discrete-time representation [24]. We then truncate this time-domain precoder to the number of RB considered (viz. 4 and 8). This time-domain precoder is then quantised and tracked, and is fed back to the transmitter to reconstruct the complete precoder for all subcarriers.

In our approach that uses the lattice structure parameters, a time domain matrix all-pass filter is first computed at the receiver using a different set of pilot subcarriers depending on the filter order (equi-spaced), and then represented using lattice structure parameters. These lattice structure parameters are subsequently tracked by applying feedback on the  $\mathcal{K}_k$  parameters, as described in Section III-C. The parameters considered for the simulations are shown in TABLE II.

We first consider a slowly varying channel, as described in (5) and (6) for typical speeds  $v \in \{10, 50, 100\}$  km/h, and  $T_s \approx 75 \mu s$ . We use the adaptive quantisation as per (18) to track the precoder for both geodesic and lattice methods, wherein the parameter  $\sigma$  is tuned optimally, depending on the speed. As shown in Table II, the geodesic and Givens parameters based approaches employ precoder interpolation from the

TABLE II  
SIMULATION PARAMETERS

<b>MIMO System</b>	<b><math>4 \times 4</math></b>	<b><math>8 \times 8</math></b>	<b><math>12 \times 12</math></b>	<b><math>15 \times 15</math></b>
<b>Total subcarriers (<math>N_{sc}</math>)</b>	4096			
<b>Pilot subcarriers (<math>N_p</math>)</b>	4	4	8	8
<b>Total feedback bits (Geodesic)</b>	128	512	2304	3600
<b>Total feedback bits (Givens)</b>	64	256	1152	1800
<b>Lattice filter order (<math>N_{ord}</math>)</b>	3	5	7	7
<b>Total feedback bits (Lattice)</b>	96	640	2016	3150

quantised precoders from four pilot subcarrier locations for the  $4 \times 4$  and  $8 \times 8$  systems, and eight subcarrier locations for larger MIMO configurations. In all the cases, we note that the lattice based approach requires a significantly smaller number of parameters and lower feedback, owing to the fact that they capture the precoder characteristics in a more compact manner. This is confirmed when we observe the convergence of the filter parameters by viewing the precoder adaptation error, as shown in Fig. 6, and the estimated precoder error, over time, as shown in Fig. 7; and across subcarriers as shown in Fig. 8.

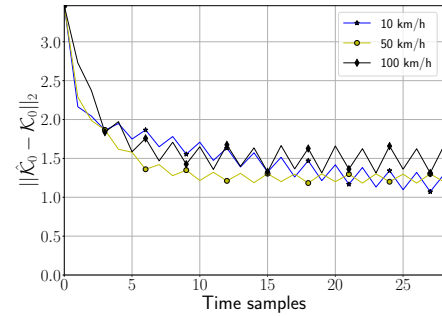


Fig. 6. Error in the estimated  $\hat{\mathcal{K}}$  for  $12 \times 12$  precoder matrices for speeds 10, 50, and 100 km/h.

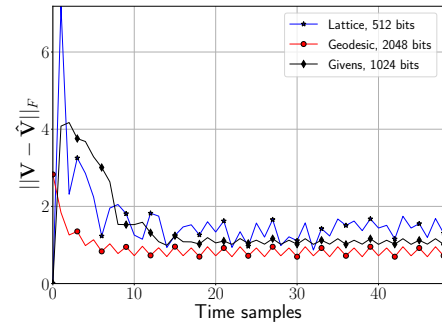


Fig. 7. Comparison of the difference between the actual and estimated precoders using the Lattice, Geodesic, and Givens methods for an  $8 \times 8$  MIMO system for speed 50 km/h.

To further highlight the effectiveness of the proposed lattice based approach to track the precoder for these channels, we have presented the performance of this approach with multiple levels of feedback, viz. 64 and 96 bits per OFDM frame in the  $4 \times 4$  situation depicted in Fig. 9a, 384 to 708 bits per OFDM frame for the  $8 \times 8$  situation in Fig. 9b, 864 to 2016 bits per OFDM frame in the  $12 \times 12$  situation in Fig. 9c, and 1350 to 3150 bits per OFDM frame for the  $15 \times 15$  situation in Fig. 9d; where the larger feedback requirement can be ascribed to the presence of more antennas. It is evident



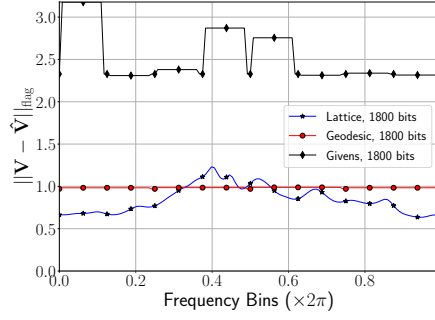


Fig. 8. Comparison of the flag distance between the actual and estimated precoders using the Lattice, Geodesic, and Givens methods for a  $15 \times 15$  MIMO system for speed 50 km/h across all subcarriers in  $[0, 2\pi]$ .

that the lattice based approach is able to track the precoders nearly as well as the Geodesic and Givens parameter based approaches with a much smaller feedback requirement (up to 70% lower than the geodesic and competitive with the Givens based approaches) with no loss in performance. In fact, with a similar feedback budget, the proposed lattice filter based channel tracking achieves higher rates. Although the error, as measured in terms of the Frobenius norm as in Fig. 7 and in terms of flag distance as in Fig. 8, for the proposed approach seems marginally higher, we note below that this does not affect the achievable rates significantly.

Due to the gradual variation of the channel, the parameters converge close to the actual values after approximately 20 adaptation steps. Here, we remark that the Givens rotation based approach experiences a higher initial error, since the scalar parameters therein are adapted independently, although it converges to the minimum error in conjunction with the other approaches. We remark that, the number of bits fed back to the transmitter is significantly lower for the lattice structure, compared to Geodesic, Givens, and angle-delay methods.

Using these adapted parameters, we now compute the achievable rate as per (8). The corresponding achievable rates for different speeds and different MIMO systems are shown in Fig. 9. First, Fig. 9a considers a  $4 \times 4$  system where with a relative speed of 10 km/h. First, since the channel variation is low, all methods are able to adapt and track the channel well. However, we observe a significant gap between in the achievable rates with the quantised channels and the perfectly precoded ones. This can be attributed to the fact that, even slight variations in the precoder could result in inefficient beamforming that reduces the rate when using linear receivers [29]. Nevertheless, we find that that lattice based approach captures the channel characteristics well, and is able to nearly match the Givens rotation based channel tracking, with only 0.3 dB separation. In the case of Fig. 9b, we have a situation where the MIMO system has more antennas ( $8 \times 8$ ), and the speed is also higher at 50 km/h. Here, we find that the lattice based approach is able to track the channel much more accurately with fewer bits than the Geodesic and the Givens methods. This is because the lattice based parameterisation is able to “capture” the 5G channel’s phase (unitary) parameters much better than the other approaches. The 5G channel typically exhibits less of a multipath and more of a strong line of sight behaviour [31] that makes

knowledge of phase more important across frequency, and representation of this unitary valued phase’s variation across frequency is better achieved by means of a matrix all-pass filter. Further, adaptation using a smaller number of lattice parameters  $\mathcal{K}_k$  (due to the lower order of the required all-pass filter) is sufficient to achieve rates comparable to the other methods (12.5% less feedback than the Givens approach while outperforming it by about 0.4 dB).

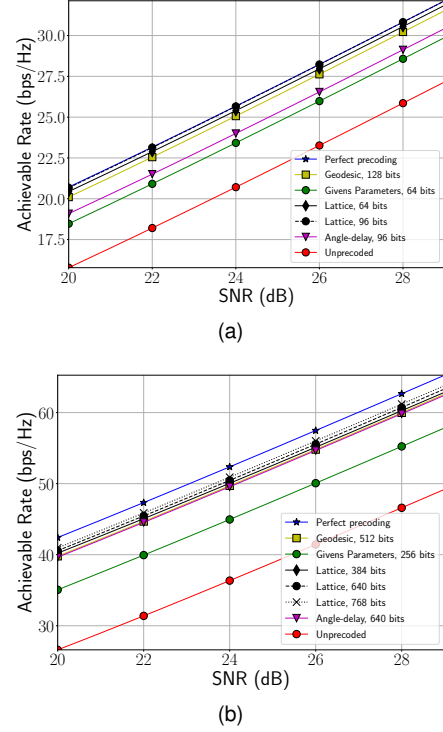


Fig. 9. Comparison of achievable rates between the lattice structure and geodesic interpolation approaches for (a)  $4 \times 4$  size precoder for relative transmitter-receiver speed 10 km/h, (b)  $8 \times 8$  size precoder for relative transmitter-receiver speed 50 km/h.

For the  $12 \times 12$  and  $15 \times 15$  channel sizes, that are more representatives of the antenna array scenarios in 5G based systems, we can again confirm the benefits of the proposed approach in Fig. 9c and Fig. 9d. In these situations, since we have a wideband OFDM system, interpolating the precoders over a wide band of frequencies using both the geodesic as well as the Givens rotations accrues a significant amount of error. Thus, at subcarriers that are far away from the pilot locations where the precoders are estimated and fed back, the error in the precoder interpolation results in inefficient beamforming, thereby reducing the rate. However, the reasonably sparse nature of the channel produces an all-pass filter that can be represented more accurately using the SNIP approach, even in situations where the number of antennas is large. Therefore, choosing a much smaller number of pilot subcarriers, and employing the SNIP is able to capture the precoder characteristics well even at the points in between the selected subcarriers. In all of these, tracking  $\mathcal{K}_k$  is also accomplished efficiently, as is confirmed in Fig. 9d.

A similar observation can be made when comparing the performance of the proposed method with the angle-delay method [24]. The angle-delay method uses a truncated



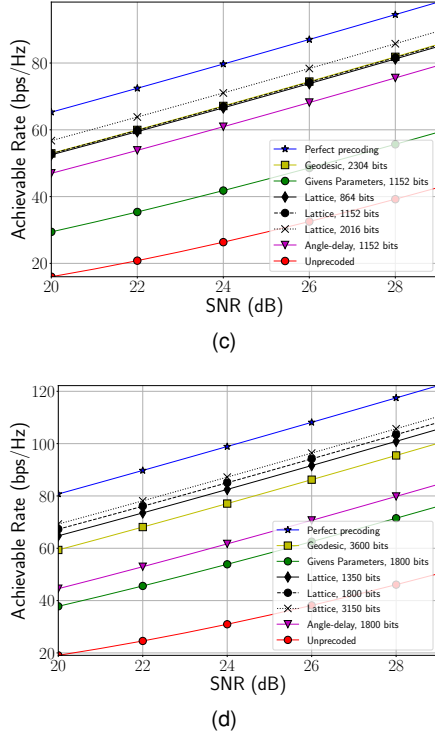


Fig. 9. Comparison of achievable rates between lattice structure and geodesic interpolation for (c)  $12 \times 12$  size precoder for relative receiver speed 50 km/h, (d)  $15 \times 15$  size precoder for relative transmitter-receiver speed 100 km/h.

discrete-time response that heavily approximates the overall precoder. We then quantise and track this approximated response, and feed it back to the transmitter. In contrast, the proposed method models the precoder through the coefficients of a matrix IIR all-pass filter, and further converts them to the lattice structure, that is suitable for quantisation and tracking while retaining the all-pass structure. This obviates the need for any time-domain approximations that are necessary in the case of the angle-delay method. Therefore, because of the combined effect of the approximate discrete-time representation and quantisation, the overall achievable-rate is lower than that achieved by the proposed method. This is seen in Fig.9a, Fig.9b, Fig.9c, and Fig.9d.

To summarise, frequency interpolation based methods, such as the geodesic and Givens rotation based approaches produce diminished performance in terms of achievable rate for larger MIMO systems owing to the larger number of parameters that need to be interpolated across subcarriers. The SNIP, on the other hand, tries to match the filter response and fit an appropriate matrix all-pass filter that yields the desired frequency response with a much smaller number of interpolating points. Thus, the combined benefit of efficient representation of the filter and convenient adaptive tracking makes the SNIP based approach an attractive proposition for precoder tracking in 5G MIMO communication systems.

## V. CONCLUSION

In this work we emphasis on lattice based time-domain realisation of a matrix all-pass filter and present its practicality for designing precoders for MIMO-OFDM systems. We use the optimised SNIP to obtain the matrix LCCDE filter coefficients and then convert them to matrix lattice parameters for

convenient representation. By doing so, we obtain the inherent benefits of the lattice structure: *stability* and *adaptability*. We show that our proposed structure is on par with the conventional (frequency-domain) geodesic and Givens rotation approaches, and angle-delay domain approach in terms of 1) better adaptation, 2) comparable achievable data-rates, and 3) smaller number of feedback bits. Future work would explore more effective techniques for estimating precoders directly in the lattice form, and the applicability of the proposed techniques in MIMO joint radar and communication systems.

## REFERENCES

- [1] M. A. Albreem, A. H. Al Habbash, A. M. Abu-Hudrouss, and S. S. Ikki, "Overview of precoding techniques for massive MIMO," *IEEE Access*, vol. 9, pp. 60 764–60 801, 2021.
- [2] S. Domouchtsidis, C. Tsinos, S. Chatzinotas, and B. Ottersten, "Constant envelope massive MIMO-OFDM precoding: An improved formulation and solution," in *ICASSP 2020-2020 IEEE International Conference on Acoustics, Speech and Signal Processing (ICASSP)*. IEEE, 2020, pp. 8956–8960.
- [3] M. Yao, M. Carrick, M. M. Sohel, V. Marojevic, C. D. Patterson, and J. H. Reed, "Semidefinite relaxation-based PAPR-aware precoding for massive MIMO-OFDM systems," *IEEE Transactions on Vehicular Technology*, vol. 68, no. 3, pp. 2229–2243, 2018.
- [4] N. Fatema, G. Hua, Y. Xiang, D. Peng, and I. Natgunanathan, "Massive MIMO linear precoding: A survey," *IEEE Systems Journal*, vol. 12, no. 4, pp. 3920–3931, 2017.
- [5] D. S. Baum, J. Hansen, J. Salo, G. Del Galdo, M. Milojevic, and P. Kyösti, "An interim channel model for beyond-3g systems: extending the 3gpp spatial channel model (scm)," in *2005 IEEE 61st Vehicular Technology Conference*, vol. 5. IEEE, 2005, pp. 3132–3136.
- [6] Y. d. J. Bultitude and T. Rautiainen, "Ist-4-027756 winner ii d1. 1.2 v1. 2 winner ii channel models," *EBITG, TUI, UOULU, CU/CRC, NOKIA, Tech. Rep*, 2007.
- [7] B. Mondal, T. A. Thomas, E. Visotsky, F. W. Vook, A. Ghosh, Y.-H. Nam, Y. Li, J. Zhang, M. Zhang, Q. Luo *et al.*, "3d channel model in 3gpp," *IEEE Communications Magazine*, vol. 53, no. 3, pp. 16–23, 2015.
- [8] T. Ghirmai, "Design of reduced complexity feedback precoding for MIMO-OFDM," *International Journal of Communication Systems*, vol. 29, no. 1, pp. 142–154, 2016.
- [9] S. Guo, C. Xing, Z. Fei, and D. Li, "Robust capacity maximization transceiver design for MIMO OFDM systems," *Science China Information Sciences*, vol. 59, no. 6, pp. 1–11, 2016.
- [10] B. Gupta, S. Gupta, A. K. Singh, and H. D. Joshi, "Optimised periodic precoder-based blind channel estimation for MIMO-OFDM systems," *International Journal of Electronics Letters*, vol. 6, no. 3, pp. 347–363, 2018.
- [11] O. Taghizadeh, V. Radhakrishnan, A. C. Ciriki, S. Shojaei, R. Mathar, and L. Lampe, "Linear precoder and decoder design for bidirectional Full-Duplex MIMO OFDM systems," in *2017 IEEE 28th Annual International Symposium on Personal, Indoor, and Mobile Radio Communications (PIMRC)*. IEEE, 2017, pp. 1–5.
- [12] S. Wu, C.-X. Wang, M. M. Alwakeel, X. You *et al.*, "A general 3-d non-stationary 5g wireless channel model," *IEEE Transactions on Communications*, vol. 66, no. 7, pp. 3065–3078, 2017.
- [13] J. Bian, C.-X. Wang, X. Gao, X. You, and M. Zhang, "A general 3d non-stationary wireless channel model for 5g and beyond," *IEEE Transactions on Wireless Communications*, vol. 20, no. 5, pp. 3211–3224, 2021.
- [14] S. Nijhawan, A. Gupta, K. Appaiah, R. Vaze, and N. Karamchandani, "Flag manifold-based precoder interpolation techniques for mimo-ofdm systems," *IEEE Transactions on Communications*, vol. 69, no. 7, pp. 4347–4359, 2021.
- [15] D. J. Love and R. W. Heath, "Grassmannian precoding for spatial multiplexing systems," in *PROCEEDINGS OF THE ANNUAL ALLERTON CONFERENCE ON COMMUNICATION CONTROL AND COMPUTING*, vol. 41, no. 1. The University; 1998, 2003, pp. 356–357.
- [16] B. E. Godana and T. Ekman, "Parametrization based limited feedback design for correlated mimo channels using new statistical models," *IEEE Transactions on Wireless Communications*, vol. 12, no. 10, pp. 5172–5184, 2013.

- [17] X. Liu, H.-H. Chen, X. Wang, and W. Meng, "Time domain precoding for OFDM/OFDMA systems without cyclic prefix," *IEEE Transactions on Vehicular Technology*, vol. 67, no. 6, pp. 5510–5514, 2018.
- [18] N. Solomennikova, A. Sherstobitov, and V. Lyshev, "Frequency Selective MIMO precoding in Time Domain," in *2021 International Conference Engineering and Telecommunication (En&T)*. IEEE, 2021, pp. 1–6.
- [19] P. A. Regalia, S. K. Mitra, and P. Vaidyanathan, "The digital all-pass filter: A versatile signal processing building block," *Proceedings of the IEEE*, vol. 76, no. 1, pp. 19–37, 1988.
- [20] P. Vaidyanathan and S. Mitra, "A general family of multivariable digital lattice filters," *IEEE Transactions on Circuits and Systems*, vol. 32, no. 12, pp. 1234–1245, 1985.
- [21] P. Vaidyanathan and Z. Doganata, "The role of lossless systems in modern digital signal processing: A tutorial," *IEEE Transactions on Education*, vol. 32, no. 3, pp. 181–197, 1989.
- [22] P. Vaidyanathan and S. K. Mitra, "A unified structural interpretation of some well-known stability-test procedures for linear systems," *Proceedings of the IEEE*, vol. 75, no. 4, pp. 478–497, 1987.
- [23] A. S. Bharath, D. S. Gaharwar, K. Appaiah, and D. Pal, "Design of discrete-time matrix all-pass filters using subspace nevanlinna pick interpolation," 2022. [Online]. Available: <https://arxiv.org/abs/2210.14015>
- [24] J. Mo, P. Schniter, and R. W. Heath, "Channel Estimation in Broadband Millimeter Wave MIMO Systems with Few-Bit ADCs," *IEEE Transactions on Signal Processing*, vol. 66, no. 5, pp. 1141–1154, 2017.
- [25] N. Khaled, R. W. Heath, G. Leus, B. Mondal, and F. Petré, "Interpolation-based multi-mode precoding for mimo-ofdm systems," in *2005 13th European Signal Processing Conference*. IEEE, 2005, pp. 1–4.
- [26] J. C. Roh and B. D. Rao, "Efficient feedback methods for MIMO channels based on parameterization," *IEEE Transactions on Wireless Communications*, vol. 6, no. 1, pp. 282–292, 2007.
- [27] M. Madan, A. Gupta, and K. Appaiah, "Scalar feedback-based joint time-frequency precoder interpolation for mimo-ofdm systems," *IEEE Wireless Communications Letters*, vol. 9, no. 9, pp. 1562–1566, 2020.
- [28] T. Kim, D. J. Love, and B. Clerckx, "MIMO systems with limited rate differential feedback in slowly varying channels," *IEEE Transactions on Communications*, vol. 59, no. 4, pp. 1175–1189, 2011.
- [29] R.-A. Pitaval, A. Srinivasan, and O. Tirkkonen, "Codebooks in flag manifolds for limited feedback mimo precoding," in *SCC 2013; 9th International ITG Conference on Systems, Communication and Coding*. VDE, 2013, pp. 1–5.
- [30] D. J. Love and R. W. Heath, "Multimode precoding for mimo wireless systems," *IEEE Transactions on Signal Processing*, vol. 53, no. 10, pp. 3674–3687, 2005.
- [31] M. K. Samimi and T. S. Rappaport, "3-D Millimeter-wave Statistical Channel Model for 5G Wireless System Design," *IEEE Transactions on Microwave Theory and Techniques*, vol. 64, no. 7, pp. 2207–2225, 2016.
- [32] X. Gao, L. Dai, S. Han, I. Chih-Lin, and R. W. Heath, "Energy-efficient hybrid analog and digital precoding for mmWave MIMO systems with large antenna arrays," *IEEE Journal on Selected Areas in Communications*, vol. 34, no. 4, pp. 998–1009, 2016.
- [33] H. Miao and M. Faerber, "Physical Downlink Control Channel for 5G New Radio," in *2017 European conference on networks and communications (EuCNC)*. IEEE, 2017, pp. 1–5.